Check for updates

OPEN

Structural dynamics of $CH_3NH_3^+$ and $PbBr_3^-$ in tetragonal and cubic phases of $CH_3NH_3PbBr_3$ hybrid perovskite by nuclear magnetic resonance

Ae Ran Lim[1✉], Sun Ha Kim[2,3] & Yong Lak Joo[4]

Understanding the structural dynamics of lead-halide perovskites is essential for their advanced use as photovoltaics. Here, the structural dynamics of the CH_3NH_3 cation and $PbBr_6$ octahedra in the perovskite $CH_3NH_3PbBr_3$ were studied via nuclear magnetic resonance (NMR) to determine the mechanism of the transition from the tetragonal to cubic phase. The chemical shifts were obtained by ^1H, ^{13}C, and ^{207}Pb magic angle spinning NMR and ^{14}N static NMR. The chemical shifts of the ^1H nuclei in CH_3 and NH_3 remained constant with increasing temperature, whereas those of the ^{13}C and ^{207}Pb nuclei varied near the phase transition temperature ($T_C = 236$ K), indicating that the structural environments of ^{13}C and ^{207}Pb change near T_C. The spin–lattice relaxation time $T_{1\rho}$ values for ^1H, ^{13}C, and ^{207}Pb nuclei increased with increasing temperature and did not exhibit an abrupt change near T_C. In addition, the two lines in the ^{14}N NMR spectra superposed into one line near T_C, indicating the occurrence of a phase transition to a cubic phase with higher symmetry than tetragonal. Consequently, the main factor causing the phase transition from the tetragonal to cubic phase near T_C is a change in the surroundings of the ^{207}Pb nuclei in the $PbBr_6$ octahedra and of the C–N groups in the CH_3NH_3 cations.

Lead-halide perovskites currently represent the most promising photovoltaic materials for the production of low-cost, high-performance solar cells[1,2]. In recent years, researchers have succeeded in significantly improving the power conversion efficiency (PCE) of this hybrid perovskite, and rapid advances in this field led to a record-high PCE. The very important for optoelectronic heterostructures are solar cells, photodetectors, and laser diodes[3–6]. For this class of materials, which has the general formula $CH_3NH_3PbX_3$ (X = Cl, Br, and I), an inorganic cage of PbX_6 octahedra encloses an organic cation at the $CH_3NH_3^+$ site[7–12]. The phase transition temperatures of $CH_3NH_3PbBr_3$, a representative perovskite, are 148.8, 154, and 236.3 K, corresponding to a total of four crystal phases[13,14]; with decreasing temperature, the cubic phase (I) transforms to a tetragonal phase (II) at 236.3 K, to another tetragonal phase (III) at 154 K, and finally to an orthorhombic phase (IV) at 148.8 K. In tetragonal phase II, the $CH_3NH_3^+$ ions undergo isotropic reorientation, whereas in the lower-temperature phases, the reorientation of C–N axes seems to be frozen[15]. All the phase transitions are first-order and order–disorder type, although the highest temperature transition is close to second-order. From the high-temperature cubic phase with freely rotating CH_3NH_3 cations, this compound enters lower-symmetry tetragonal phases and finally a low-temperature orthorhombic phase with the orientation of CH_3NH_3 cations fixed at ordered positions[16–20]. At room temperature, the structure is cubic, the space group is Pm3m, and the lattice constant $a = 5.93129$ Å and $Z = 1$[13]. In this crystal structure, there exists a $CH_3NH_3^+$ cation at the centre of a cube formed by corner-sharing $PbBr_6$ octahedra[18,21], as shown in Fig. 1. Below 236 K, the crystal structure has a tetragonal and belongs to the space group I4/mcm with lattice constants $a = b = 8.32$ Å, $c = 11.83$ Å, and $Z = 4$[22]. Throughout the transition

[1]Analytical Laboratory of Advanced Ferroelectric Crystals, Department of Science Education, Jeonju University, Jeonju 55069, Korea. [2]Seoul Western Center, Korea Basic Science Institute, Seoul 03759, Korea. [3]Department of Chemistry, Kyungpook National University, Daegu 41566, Korea. [4]Robert Fredrick Smith School of Chemical and Biomolecular Engineering, Cornell University, Ithaca, NY 14853, USA. ✉email: aeranlim@hanmail.net

1
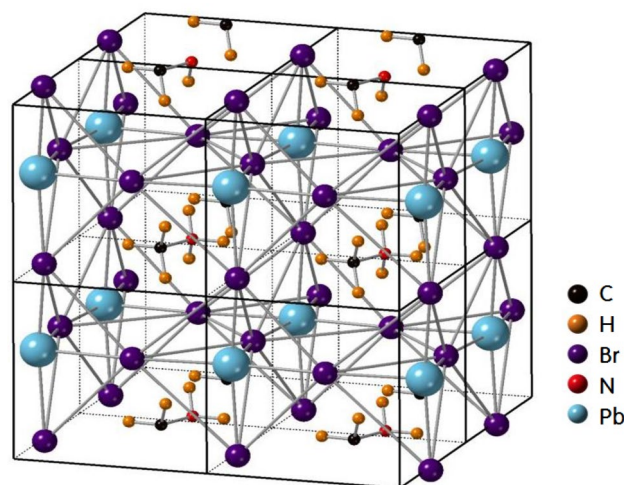
Figure 1. Crystal structure of cubic phase $CH_3NH_3PbBr_3$. The software used to create the Fig. is CrystalMaker Software.

from the tetragonal II phase to the tetragonal III phase at 154 K, the full width at half maximum of the Raman ν_6 band shows an abrupt increase[8]. At lower temperatures, $CH_3NH_3PbBr_3$ undergoes a first-order structural phase transition from the tetragonal III (I4/mmm) phase to the orthorhombic IV (Pnma) phase[9].

In a previous nuclear magnetic resonance (NMR) investigation, the temperature dependence of ^{81}Br nuclear quadrupole resonance frequencies and ^1H spin–lattice relaxation times in the laboratory frame T_1 for $CH_3NH_3PbBr_3$ were discussed by Xu et al.[23] According to their results, the two ^{81}Br NQR lines in phase II were reduced to one line in phase I. The discontinuity of the NQR line at this transition point implied a first-order transition. ^1H T_1 varied continuously, and no discernible change in the free induction decay was observed during the I–II transition. The phase transition had no significant effect on the motional state of the $CH_3NH_3^+$ ions. Furthermore, Baikie et al.[13] reported that the ^1H magic angle spinning (MAS) NMR spectra showed two clear peaks corresponding to the CH_3 and NH_3 environments in the high-temperature phase, and the ^1H and ^{13}C NMR spectra of $CH_3NH_3PbBr_3$ showed that the $CH_3NH_3^+$ units undergo dynamic reorientation.

Measuring the spin–lattice relaxation time in the rotating frame $T_{1\rho}$ by MAS NMR allows for the probing of molecular motion in the kHz range, whereas the spin–lattice relaxation time in the laboratory frame T_1 measured by static NMR reflects motion in the MHz range. Although the ^1H T_1 of $CH_3NH_3PbBr_3$ has been examined by a few research groups, the corresponding phenomena by ^1H, ^{13}C, and ^{207}Pb MAS NMR spectra and $T_{1\rho}$ have not been fully studied. In addition, information regarding ^{14}N in the CH_3NH_3 cation has not yet been discussed.

In the present study, the structural dynamics of the CH_3NH_3 cation and $PbBr_6$ octahedra in $CH_3NH_3PbBr_3$ were studied in detail by NMR to resolve the phase transition mechanisms from the tetragonal phase to the higher-temperature cubic phase. The temperature dependences of the chemical shifts and spin–lattice relaxation time in the rotating frame $T_{1\rho}$ were measured using ^1H MAS NMR, ^{13}C cross-polarization (CP)/MAS NMR, and ^{207}Pb MAS NMR with emphasis on the role of the CH_3NH_3 cation and $PbBr_6$ octahedra in $CH_3NH_3PbBr_3$. In addition, the ^{14}N static NMR spectra of $CH_3NH_3PbBr_3$ in the laboratory frame were acquired near the phase transition temperature. The abovementioned results help in understanding the thermal stability and the structural dynamics based on the phase transition mechanism, towards the practical application of this material.

Experimental

CH_3NH_3Br and $PbBr_2$ were dissolved in a dimethylformamide solution and heated the mixed suspension on a hot plate to obtain a transparent solution. Detailed methods for the crystal growth are given elsewhere[21,24,25]. The $CH_3NH_3PbBr_3$ single crystals obtained here were orange in colour with a square shape.

Differential scanning calorimetry (DSC) (TA, DSC 25) was conducted at a heating rate of 10 °C/min over a temperature range from 190 to 525 K under nitrogen gas. Thermogravimetric analysis (TGA) was performed on a thermogravimetric analyser (TA Instrument) in an interval from 300 to 780 K at a heating rate of 10 °C/min. Approximately 11.15 mg of $CH_3NH_3PbBr_3$ was used in each experiment.

NMR measurements were carried out at 9.4 T using a Bruker 400 MHz Avance II + spectrometer at the Korea Basic Science Institute, Western Seoul Center. The ^1H, ^{13}C, and ^{207}Pb NMR frequencies were 400.13, 100.61, and 83.75 MHz, respectively. Powdered samples were packed in zirconia MAS rotors with Macor caps, and the MAS rate was set to 10 kHz for the ^1H MAS, ^{13}C MAS, and ^{207}Pb MAS NMR measurements to minimise spinning sideband overlap. The spin–lattice relaxation time in the rotating frame $T_{1\rho}$ was measured using an inversion recovery pulse sequence, which employs compensating pulses. The ^{13}C $T_{1\rho}$ values were measured by varying the duration of the ^{13}C spin-locking pulse applied after the CP preparation period. The width of the $\pi/2$ pulse used for measuring $T_{1\rho}$ of ^1H and ^{13}C was 3.45 μs, and that for measuring $T_{1\rho}$ of ^{207}Pb was 3.5 μs. In addition,
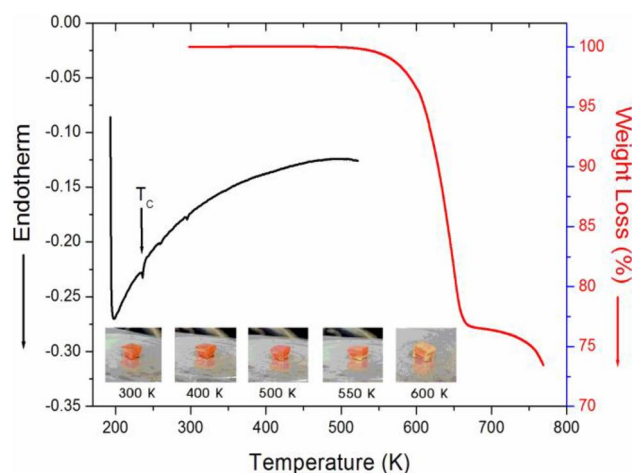
Figure 2. Differential scanning calorimetry (DSC) and thermogravi-metric analysis (TGA) of $CH_3NH_3PbBr_3$ (inset: color changes of $CH_3NH_3PbBr_3$ single crystal according to the temperature).
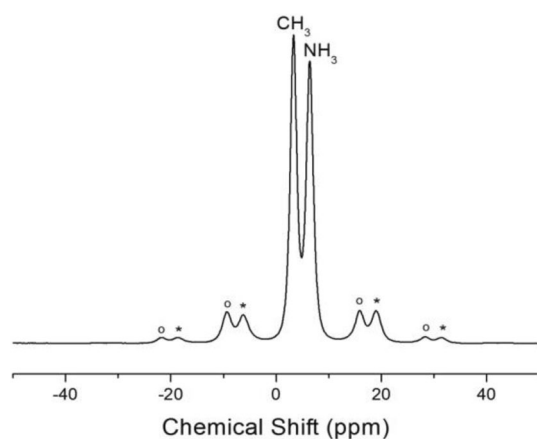
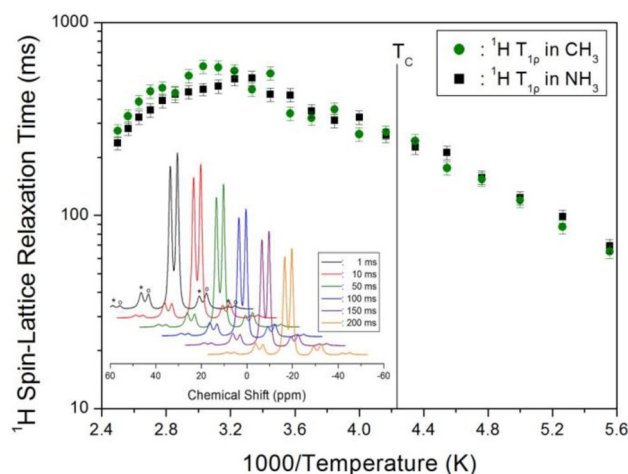**Figure 3.** ^1H MAS NMR spectrum for CH_3 and NH_3 of $CH_3NH_3PbBr_3$ at 300 K, and the spinning sidebands are marked with open circles and asterisks.

^{14}N NMR spectra of a $CH_3NH_3PbBr_3$ single crystal were measured with a Larmor frequency of 28.90 MHz in the laboratory frame.

Temperature-dependent NMR spectra were recorded over 180 to 430 K; the NMR spectra and relaxation times could not be measured outside this temperature range because of the limitations of the spectrometer. Sample temperatures were held constant within ± 0.5 K by controlling the nitrogen gas flow and heating current.

Experimental results

Figure 2 shows the DSC and TGA curves obtained under a nitrogen atmosphere. DSC analysis was used to determine the phase transition temperature; only one endothermic peak related to a phase transition was observed at 236 K, which is consistent with previously reported T_C values.[13,14] The thermal stability of $CH_3NH_3PbBr_3$ was examined by TGA. The first occurrence of mass loss began at approximately 530 K, which represents the onset of partial thermal decomposition. The mass sharply decreased between 550 and 650 K, with a corresponding mass loss of 22% near 650 K. Optical polarizing microscopy experiments were also conducted to further understand the thermal stability at high temperatures. The colour of the crystal was orange at room temperature, as shown in the inset in Fig. 2. As the temperature increased, the state of the crystal remained the same from 400 to 500 K. Above 550 K, a slight opacity occurred at the bottom of the crystal, and at approximately 600 K, the crystal was nearly opaque.

The ^1H NMR spectrum of $CH_3NH_3PbBr_3$ was recorded by MAS NMR at a frequency of 400.13 MHz. Figure 3 shows the ^1H MAS NMR spectrum at 300 K, where the spinning sidebands are marked with open circles and asterisks. The two peaks in the ^1H spectrum correspond to CH_3 and NH_3 environments, with the chemical shifts at $\delta = 3.27$ and 6.36 ppm assigned to ^1H in CH_3 and NH_3, respectively. The chemical shifts remained quasi-constant with increasing temperature, indicating that the structural environments of ^1H in the CH_3 and

Figure 4. ^{1}H spin–lattice relaxation times $T_{1\rho}$ for the CH_3 and NH_3 ions of $CH_3NH_3PbBr_3$ as a function of inverse temperature (inset: recovery plots of the ^{1}H MAS NMR spectrum by delay time at 300 K).

NH_3 groups were unchanged (see the Supplementary Information). Additionally, the line width (full-width at half-maximum) of the ^{1}H MAS NMR signal at 300 K is approximately 1.62 ppm, which also remained nearly constant with temperature change.

The ^{1}H inversion-recovery curves for both CH_3 and NH_3 at each temperature were fitted to exponentials to extract $T_{1\rho}$. The data were well fitted a single exponential, indicating that there is one dominant relaxation mechanism acting per environment. Thus, $T_{1\rho}$ was determined by fitting the decay plots with the equation below[26,27].

$$P(t)/P_0 = \exp\left(-t/T_{1\rho}\right), \tag{1}$$

where $P(t)$ is the magnetisation, t is the spin-locking pulse duration, and P_0 is the total nuclear magnetisation of ^{1}H at thermal equilibrium. The recovery curves of ^{1}H in $CH_3NH_3PbBr_3$ were measured for various delay times at each temperature. Figure 4 (inset) shows the recovery traces for ^{1}H measured for delay times ranging from 1 to 200 ms at 300 K. The intensity of the recovery traces differed with delay time. The $T_{1\rho}$ values obtained from the intensity versus delay time and shown in Fig. 4 reveal that $T_{1\rho}$ increased with temperature because proton hopping was accelerated. This is in agreement with Xu et al.[23], who reported that the ^{1}H T_1 increased smoothly with increasing temperature through the high-temperature phase transition. The $T_{1\rho}$ values of ^{1}H in CH_3 and NH_3 in the $CH_3NH_3^+$ cation show similar trends with temperature and are nearly the same within the error range. The $T_{1\rho}$ values show no change near the phase transition temperature ($T_C = 236$ K). $T_{1\rho}$ increased with increasing temperature, reaching the maximum values of 592 ms and 456 ms for CH_3 and NH_3, respectively, near 330 K above the phase transition temperature, and then decreased with increasing temperature. Although the structural environment of ^{1}H in the CH_3NH_3 groups does not change with temperature, their molecular motion increases at high temperatures, as indicated by the $T_{1\rho}$ values. Above T_C, the ^{1}H $T_{1\rho}$ value for CH_3 slightly exceed that for NH_3.

Structural analysis of the ^{13}C and ^{207}Pb nuclei in $CH_3NH_3PbBr_3$ was performed by MAS NMR, and the corresponding spectra at 300 K are shown as insets in Fig. 5. At room temperature, the ^{13}C and ^{207}Pb MAS NMR spectra show one signal each at chemical shifts of $\delta = 30.66$ and 89 ppm with respect to tetramethylsilane and $PbNO_3$, respectively. Here, the line width for ^{13}C at 300 K is narrow at 2.77 ppm, whereas that for ^{207}Pb is quite broad at 206.24 ppm. Figure 5 shows the ^{13}C and ^{207}Pb chemical shifts of $CH_3NH_3PbBr_3$ measured as a function of temperature, illustrating that the ^{13}C and ^{207}Pb peak positions moved to higher chemical shifts upon heating. The chemical shifts near T_C changed, in contrast to the ^{1}H chemical shifts. The chemical shifts of the ^{13}C and ^{207}Pb signals relative to the reference signal are sensitive to the electronic environment of the nucleus. In particular, the ^{207}Pb chemical shift changed more rapidly than that of ^{13}C near T_C. From these results, the phase transition from the tetragonal to cubic phase is thought to arise from a change in the $PbBr_6$ octahedra.

To determine the $T_{1\rho}$ values of ^{13}C and ^{207}Pb in the rotating frame, the nuclear magnetisation was measured as a function of delay time. The signal intensities of the nuclear magnetisation recovery curves could be described by the single exponential function in Eq. (1), and the signal intensity followed this single exponential decay at all temperatures. From these results, the $T_{1\rho}$ values were obtained for ^{13}C and ^{207}Pb in $CH_3NH_3PbBr_3$ as a function of inverse temperature, as shown in Fig. 6. The ^{13}C and ^{207}Pb $T_{1\rho}$ values for CH_3 and $PbBr_3$ seem to follow a similar trend with temperature to that of the ^{1}H $T_{1\rho}$, where the values increase with increasing temperature and are approximately continuous near T_C. In addition, the ^{207}Pb $T_{1\rho}$ values are much lower than ^{13}C $T_{1\rho}$.

To obtain information concerning possible changes in the surroundings of the ^{14}N ion, static NMR spectra of ^{14}N ($I = 1$) in the laboratory frame were obtained. Temperature-dependent changes in the ^{14}N resonance frequency are attributable to alterations in the structural geometry, indicating a change in the quadrupole coupling constant of the ^{14}N nuclei. The spectra were obtained by the solid-state echo method using static NMR at a Larmor frequency of 28.90 MHz. Two resonance signals were expected from the quadrupole interactions of the ^{14}N nucleus with spin $I = 1$. The ^{14}N NMR spectra were shown at 225 and 270 K, and the resonance frequencies referenced
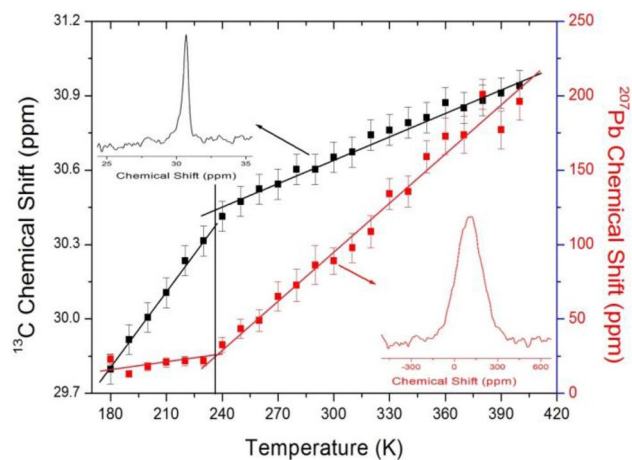
Figure 5. ^{13}C and ^{207}Pb chemical shifts in $CH_3NH_3PbBr_3$ as a function of temperature (inset: ^{13}C and ^{207}Pb MAS NMR spectrum of $CH_3NH_3PbBr_3$ at 300 K).
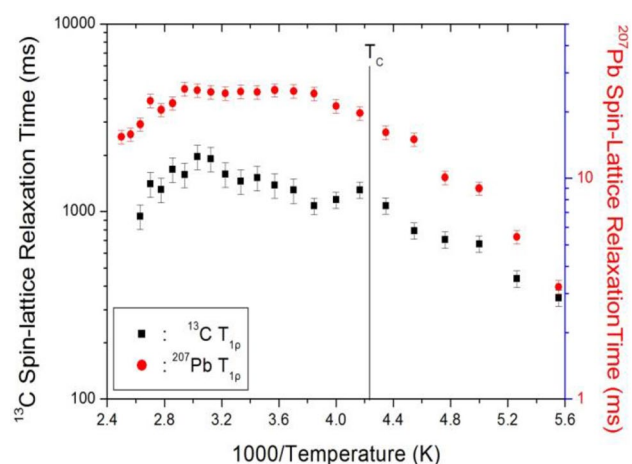

Figure 6. ^{13}C and ^{207}Pb spin–lattice relaxation times $T_{1\rho}$ of $CH_3NH_3PbBr_3$ as a function of inverse temperature.

with respect to NH_4NO_3 as a function of temperature are shown in Fig. 7. The line widths are very narrow at all temperatures. The two resonance signals for ^{14}N, which are attributable to NH_3, superpose into one line at the transition point of 236 K. This single ^{14}N resonance line indicates that a phase transition takes place to a new phase with a higher symmetry than tetragonal[28]. In tetragonal phase below T_C, the electric field gradient tensors at the N sites vary, reflecting changes in the atomic configuration around the nitrogen. But, there is no electric field gradient tensor at the ^{14}N site in the cubic structure because of the site symmetry of m3m.

Conclusion

Using the information derived from NMR studies near T_C (= 236 K), we have probed the structural and dynamic features of $CH_3NH_3PbBr_3$ in detail and demonstrated its dynamic nature. The ionic dynamics of $CH_3NH_3PbBr_3$, with emphasis on the role of the CH_3NH_3 cation and $PbBr_6$ octahedra, were investigated by ^1H MAS NMR, ^{13}C CP/MAS NMR, ^{207}Pb MAS NMR, and ^{14}N static NMR as a function of temperature. ^1H, ^{13}C, and ^{207}Pb NMR were used to identify the phase transition in $CH_3NH_3PbBr_3$ by detecting changes in the chemical shifts accompanying a change in crystallographic symmetry. Here, the CH_3 and NH_3 groups were distinguished based on the ^1H chemical shifts. The chemical shifts of the ^1H nuclei remained constant at all temperatures, whereas those of the ^{13}C and ^{207}Pb nuclei varied with temperature. The temperature dependence of the chemical shifts was sensitive to the rotation of the $PbBr_6$ octahedra. From these results, it is evident that the structural environments of ^{13}C and ^{207}Pb change near T_C. The change in ^{207}Pb chemical shift near T_C can be explained by the rotation of $PbBr_3$. This is consistent with the established nature of the phase transition. Additionally, the NMR line widths of ^1H, ^{13}C, and ^{207}Pb were 1.62, 2.77, and 206.24 ppm, respectively, and the relaxation time is proportional to the inverse of the line width. Although the chemical shifts of ^{13}C and ^{207}Pb abruptly varied near T_C, the ^1H, ^{13}C, and ^{207}Pb $T_{1\rho}$ values showed a similar trend with increasing temperature, and their $T_{1\rho}$ values were continuous near T_C. These
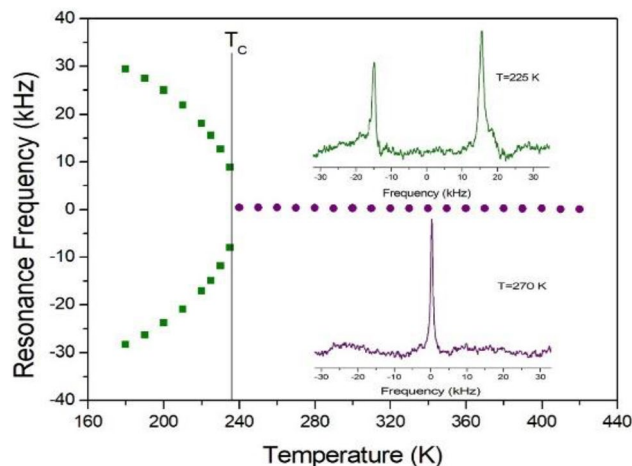
Figure 7. The ^{14}N resonance frequency of CH$_3$NH$_3$PbBr$_3$ single crystal as a function of temperature (inset: ^{14}N NMR spectrum at tetragonal phase of 225 K and cubic phase of 270 K).

short relaxation times indicate ease of molecular motion. The TGA results also showed that CH$_3$NH$_3$PbBr$_3$ has a high thermal stability.

In addition, the abrupt change occurring in the resonance frequency of the ^{14}N nuclei near T_C is attributable to a structural phase transition. The NH$_3$ groups in the structure are coordinated by PbBr$_6$, and thus atomic displacements in the environment of the ^{14}N nuclei with temperature are correlated with PbBr$_6$. The electrostatic interactions governed by hydrogen-bonding interactions between the NH$_3^+$ group in the CH$_3$NH$_3$ cation and the PbBr$_6$ octahedra play an important role in the dynamics of the CH$_3$NH$_3$ cations. Consequently, the main factor causing the phase transition from the tetragonal to cubic phase near T_C is a change in the surroundings of the ^{207}Pb nuclei in the PbBr$_6$ octahedra and in the surroundings of C–N groups in the CH$_3$NH$_3$ cations. Based on these results, the structural dynamics within the CH$_3$NH$_3$PbBr$_3$ perovskite structure are expected to have a significant effect on the operation mechanism of perovskite solar cells.

References

1. Yang, W. S. *et al.* High-performance photovoltaic perovskite layers fabricated through intramolecular exchange. *Science* **348**, 1234 (2015).
2. Brenner, T. M., Egger, D. A., Kronik, L., Hodes, G. & Cahen, D. Hybrid organic-inorganic perovskites: low-cost semiconductors with intriguing charge-transport properties. *Nat. Tev. Mater.* **1**, 15007 (2016).
3. Al-Amri, A. M., Leung, S.-F., Vaseem, M., Shamim, A. & He, J.-H. Fully inkjet-printed photodetector using a grapheme/perovskite/grapheme heterostructure. *IEEE Trans. Electron Dev.* **66**, 2657 (2019).
4. Al-Amri, A. M., Cheng, B. & He, J.-H. Perovskite methylammonium lead trihalide heterostructures: progress and challenges. *IEEE Trans. Nanotechnol.* **18**, 1 (2019).
5. Liu, W.-W. *et al.* Platinum-free ternary metallic selenides as nanostructured counter electrode for high-efficiency dye-sensitized solar cell by interface engineering. *ACS Appl. Energy Mater.* **3**, 3704 (2020).
6. Lin, C.-H. *et al.* Giant optical anisotropy of perovskite nanowire array films. *Adv. Funct. Mater.* **30**, 1909275 (2020).
7. Capitani, F. *et al.* Locking of methylammonium by pressure-enhanced H-bonding in (CH3NH3)PbBr$_3$ hybrid perovskite. *J. Phys. Chem. C* **121**, 28125 (2017).
8. Nakada, K., Matsumoto, Y., Shimo, Y., Yamada, K. & Furukawa, Y. Temperature-dependent evolution of Raman spectra of methylammonium lead halide perovskites, CH$_3$NH$_3$PbX$_3$ (X = I, Br). *Molecules* **24**, 626 (2019).
9. Swainson, I. P., Hammond, R. P., Soulliere, C., Knop, O. & Massa, W. Phase transitions in the perovskite methylammonium lead bromide, CH$_3$ND$_3$PbBr$_3$. *J. Solid State Chem.* **176**, 97 (2003).
10. Chen, Y. *et al.* Introduction of nitrogen gas flow and precursor aging process to improve the efficiency of the lead acetate derived CH$_3$NH$_3$PbI$_3$ perovskite solar cells. *Solar Energy Mater. Sol. Cells* **190**, 49 (2019).
11. Baikie, T. *et al.* A combined single crystal neutron/X-ray diffraction and solid-state nuclear magnetic resonance study of the hybrid perovskites CH$_3$NH$_3$PbX$_3$ (X = I, Br and Cl). *J. Mater. Chem. A* **1**, 5628 (2013).
12. Varadwaj, P. R., Varadwaj, A., Marques, H. M. & Yamashita, K. Significance of hydrogen bonding and other noncovalent interactions in determining octahedral tilting in the CH$_3$NH$_3$PbI$_3$ hybrid organic-inorganic halide perovskite solar cell semiconductor. *Sci. Rep.* **9**, 50 (2019).
13. Baikie, T. *et al.* A combined single crystal neutron/X-ray diffraction and solid-state nuclear magnetic resonance study of the hybrid perovskites CH$_3$NH$_3$PbX$_3$ (X = I, Br and Cl). *J. Mater. Chem. A* **3**, 9298 (2015).
14. Letoublon, A. *et al.* Elastic constants, optical phonons, and molecular relaxations in the high temperature plastic phase of the CH$_3$NH$_3$PbBr$_3$ hybrid perovskite. *J. Phys. Chem. Lett.* **7**, 3776 (2016).
15. Knop, O., Wasylishen, R. E., White, M. A., Cameron, T. S. & Van Oort, M. J. M. Alkylammonium lead halides, Part 2, CH$_3$NH$_3$PbX$_3$ (X = Cl, Br, I) perovskites: cuboctahedral halide cages with isotropic cation reorientation. *Can. J. Chem.* **68**, 412 (1990).
16. Ohmann, R. *et al.* Real-space imaging of the atomic structure of organic-inorganic perovskite. *J. Am. Chem. Soc.* **137**, 16049 (2015).

17. Poglitsch, A. & Weber, D. Dynamic disorder in methylammoniumtrihalogenoplumbates (II) observed by millimetre-wave spectroscopy. *J. Chem. Phys.* **87**, 6373 (1987).
18. Onoda-Yamamuro, N., Matsuo, T. & Suga, H. Calorimetric and IR spectroscopic studies of phase transitions in methylammonium trihalogenoplumbates (II). *J. Phys. Chem. Solids* **51**, 1383 (1990).
19. Weller, M. T., Weber, O. J., Henry, P. F., Di Pumpo, A. M. & Hansen, T. C. Complete structure and cation orientation in the perovskite photovoltaic methylammonium lead iodide between 100 and 352 K. *Chem. Commun.* **51**, 4180 (2015).
20. Leguy, A. M. A. *et al.* The dynamics of methylammonium ions in hybrid organic-inorganic perovskite solar cells. *Nat. Commun.* **6**, 7124 (2015).
21. Park, J.-S. *et al.* Electronic structure and optical properties of α-$CH_3NH_3PbBr_3$ perovskite single crystal. *J. Phys. Chem. Lett.* **6**, 4304 (2015).
22. Zu, F. *et al.* Constructing $CH_3NH_3PbI_3$ and $CH_3NH_3PbBr_3$ perovskite thin film electronic structure from single crystl band structure measurement. *J. Phys. Chem. Lett.* **10**, 601 (2019).
23. Xu, Q, Eguchi, T., Nakayama, H., Nakamura, N. & Kishita, M. Molecular motions and phase transitions in solid $CH_3NH_3PbX_3$ (X = Cl, Br, I) as studied by NMR and NQR. *Z. Naturforscha* **46**, 240 (1991).
24. Saidaminov, M. I. *et al.* High-quality bulk hybrid perovskite single crystals within minutes by inverse temperature crystallization. *Nat. Commun.* **6**, 7586 (2015).
25. Yang, Y. *et al.* Low surface recombination velocity in solution-grown $CH_3NH_3PbBr_3$ perovskite single crystal. *Nat. Commun.* **6**, 7961 (2015).
26. Lim, A. R. Ionic dynamics of the cation in organic-inorganic hybrid compound $(CH_3NH_3)_2MCl_4$ (M = Cu and Zn) by ^{1}H MAS NMR, ^{13}C CP MAS NMR, and ^{14}N NMR. *RSC Advances* **6**, 18656 (2018).
27. Abragam, A. *The Principles of Nuclear Magnetism* (Oxford University Press, Oxford, 1961).
28. Lim, A. R. & Kim, I. G. Phase transition study by using [133]Cs and [207]Pb nuclear magnetic resonance in a $CsPbCl_3$ single crystal. *J. Phys. Soc. Japan* **73**, 475 (2004).

Acknowledgements

Author contributions

A.R.L. designed the project and wrote the manuscript. S.H.K. performed NMR experiments. Y.L.J. suggested the idea and comment.

Competing interests

The authors declare no competing interests.

Additional information

Supplementary information is available for this paper at https://doi.org/10.1038/s41598-020-70128-5.

Correspondence and requests for materials should be addressed to A.R.L.

Reprints and permissions information is available at www.nature.com/reprints.

Publisher's note Springer Nature remains neutral with regard to jurisdictional claims in published maps and institutional affiliations.